Journal of Nondestructive Evaluation (2020) 39:49
https://doi.org/10.1007/s10921-020-00693-2

A New Ultrasonic Amplitude Tomography Approach, with Validation on Masonry Tuff Blocks

Domenico Camassa[1] · Anna Castellano[2] · Aguinaldo Fraddosio[1] · Mario Daniele Piccioni[1]

Received: 24 October 2019 / Accepted: 10 June 2020 / Published online: 22 June 2020

Abstract
Despite sonic and ultrasonic tomography are major NDT techniques, the resolution and the capability of these tests could be substantially improved; this, especially for masonry structures. Moreover, although waves amplitude attenuation is strictly related to the internal features and to the defects, some experimental and theoretical issues obstruct practical applications of amplitude tomography for civil structures. Indeed, almost exclusively travel time tomography is employed. Here, a new approach for ultrasonic amplitude tomography called Standardized Amplitude Tomography (SAT) is proposed. This approach is based on a suitable formulation of the theoretical model to be implemented for the tomographic reconstruction of the internal features of materials and on the employ of a special experimental tool. SAT approach is primarily meant for application to masonry structures, but its principle is applicable to concrete or timber structural elements as well. The effectiveness of SAT is discussed by means of experimental tests on Apulian tuff specimens having known internal defects. The results obtained by the new SAT approach are compared to those obtained by the ordinary amplitude tomography and by the classical travel time tomography.

Keywords NDT techniques · Ultrasonic tests · Acoustic tomography · Amplitude tomography · Masonry

1 Introduction

The availability of effective diagnostic [1] and monitoring [2] testing techniques for civil constructions is essential for acquiring appropriate knowledge of a structure in a non-destructive way [3, 4], and for providing data useful for preventing unexpected collapses and for designing effective and appropriate repairing and strengthening interventions [5].

This demand is particularly urgent in the case of historical and archaeological masonry buildings, that represent the history and the identity for many countries: thus, it is crucial to preserve this valuable heritage. The above considerations justify the increasing research interest on non-destructive tests (NDT), that play a crucial role in conservation, rehabilitation, restoration and strengthening of the architectural heritage [6]. Notice that also the preservation of ordinary masonry structures is relevant, since their large diffusion.

NDT aim at indirectly evaluating some relevant structural and morphological properties of the structure by measuring suitable parameters related to the properties to be determined [7–9], and generally provide only qualitative results. Among the large family of NDT techniques available for civil engineering structures, and in particular for masonry structures [1], a major role is played by acoustic tests. The latter, classified according to the employed wave frequency in sonic and ultrasonic tests, are based on the analysis of the propagation of acoustic waves through the material. Indeed, acoustic wave propagation is strictly related to the physical features of the propagation medium, and therefore acoustic measurements can be conveniently employed in inverse methods for the determination of the mechanical properties

✉ Anna Castellano
anna.castellano@poliba.it

Domenico Camassa
domenico.camassa@poliba.it

Aguinaldo Fraddosio
aguinaldo.fraddosio@poliba.it

Mario Daniele Piccioni
mariodaniele.piccioni@poliba.it

[1] Department of Civil Engineering Sciences and Architecture, Polytechnic University of Bari, Bari, Italy

[2] Department of Mechanics, Mathematics and Management, Polytechnic University of Bari, via Re David, 70125 Bari, Italy

of the material [10, 11]. Moreover, by exploiting the relation between changes in wave propagation properties and changes in the physical properties and in the state of the material, acoustic tests can be used also for the characterization of the damage [12], as well as for the determination of applied and residual stress [13, 14].

Tomography (from the Greek words *tomos*, "slice", and *grapho*, "writing") is an inverse method aiming at representing the internal features of an object without cutting it, that is, leaving undamaged the object under investigation. This principle has been exploited for the development of powerful diagnostic tools in several applicative fields like engineering, biomedical, archaeometry, etc., based on different physical principles (X-ray, radar waves, electrical impedance, magnetic resonance, etc.). Acoustic tomography, in particular, is based on the propagation of sonic and ultrasonic waves.

For concrete and masonry structures, as well as for timber structures, acoustic tomography is a relatively fast, reliable and inexpensive NDT technique for detecting, identifying and locating defects, inclusions, voids and cracks [4] and for mapping the internal distribution of some relevant physical and mechanical properties of a structural element. Due to the shorter wavelength, ultrasonic tomography allows for a better resolution, whereas it cannot be applied to very thick structures and/or with dispersive materials like, e.g., rubble masonry because of the high attenuation of the signals; in the latter cases, sonic tests are then preferred.

In particular, given a solid, acoustic tomography is based on a redundant number of measurements of an "observed parameter" related to acoustic wave propagation taken on the boundary and aims at reconstructing the distribution in the inner part of the domain of a certain property (called "model parameter") related to the observed parameter. In the case of acoustic tomography for concrete and masonry structures, basically two different model parameters may be reconstructed: the velocity (velocity tomography) or the attenuation (attenuation tomography) of propagating acoustic waves.

Velocity tomography, also known as travel time tomography, is based on the inversion of wave travel time (observed parameter). For attenuation tomography two different observed parameters may be considered: the decreasing of wave amplitude (amplitude tomography) or the frequency shift of the centroid of the signal's spectrum (frequency shift method).

Travel time tomography is the most common technique due to the robustness of travel time as the observed parameter and to the execution easiness. Several applications of travel time tomography on masonry structures are reported in the literature [15–18]. Travel time tomography has been also employed for assessing the effectiveness of strengthening interventions like grout injections on multi-leaf stone masonry walls [19]. Alongside the increase of the research interest in the conservation of the built heritage, recently an increasing number of studies on the capability of travel time tomography as NDT tool for masonry structures have been performed [20–22]. Also in the field of timber structures [23, 24] and reinforced concrete structures [25–27] travel time tomography is a widely employed and acknowledged diagnostic technique.

The quality of the results of travel time tomography depends on many factors: the frequency (in sonic or ultrasonic range) and the employed source, the number and the position of the measurements, the kind of experimental devices and the reconstruction algorithms [4]. Anyway, by examining the results in the literature, it is clear that for masonry structures the capability and the accuracy of travel time tomography in assessing hidden defects, voids, damage, the masonry layout and the mechanical properties of masonry could be still substantially improved [20]. Indeed, the resolution has a physical limit related to the wavelengths involved in the survey. Defects location and size can be generally resolved with decent accuracy, but the shape of defects is difficult to determine; moreover, small defects are difficult to detect in case of high attenuation materials [28].

Attenuation tomography has the advantage that the attenuation of sonic waves is more sensitive to some internal defects and features: the latter have a greater effect on the attenuation than on the propagation time. Indeed, wave attenuation represents the decay of energy as waves propagate through the material. Different materials differently absorb or attenuate the wave energy, depending on features such as density, viscosity, homogeneity. Moreover, waves are reflected by the boundaries between different materials, like those determined by discontinuities or defects [29, 30]. This, together with the sensitivity of the attenuation to saturation, porosity and permeability, motivates the interest for attenuation tomography in the geophysical field [31–33].

However, attenuation tomography is rarely applied to civil engineering structures because of some theoretical and experimental issues. From the theoretical point of view, describing the relationship between material features and wave amplitude decay is much more complex than modeling the relationship between material properties and wave velocity. Thus, amplitude data tomographic processing is more difficult. From the experimental point of view, signal amplitudes are strongly influenced by aspects unrelated to the material features like, e.g., the variability of the coupling conditions between probes and the surface of the material.

For the above-recalled issues, attenuation tomography could provide unreliable results, especially for masonry structures. Indeed, only a few attempts to apply attenuation tomography to masonry structures are reported in the literature [29, 34, 35]. On the other hand, for concrete structures, where higher frequencies can be used to the advantage of the resolution of acoustic tomographic tests,

there is relevant literature exploring the applicability of attenuation tomography [36–38]. Also the coupling problem has been faced by applying air-coupled transducers [39, 40].

However, the higher sensitivity of the attenuation to defects, voids and cracks compared to the travel time makes attenuation tomography a very interesting and promising technique and justifies further research efforts for fully exploiting its capability in the applicative field of masonry structures.

In this vein here, by following the research line started in [41], an innovative approach for ultrasonic amplitude tomography is proposed. This approach is primarily intended for applications to masonry structures, but in principle can be extended also to timber and concrete structures.

In particular, although the frequency shift method has been already applied also to masonry structures [15, 29], in this paper the attention is focalized on amplitude tomography because the frequency shift method involves an indirect, slightly more complicated approach for data interpretation. In addition, experimental procedures for amplitude tomography are very similar to those employed for the common and well-established travel time tomography.

The choice of the ultrasonic tomography instead of the sonic tomography, more diffused for historical masonry structures, is motivated by the purpose of stressing as much as possible the aspects of the sensitivity (the capability to locate small discontinuities) and the resolution (the capability to locate discontinuities that are close together and/or close to the surface). Moreover, as it will be explained in what follows, the experimental setup usually adopted for ultrasonic tests allows for better handle some amplitude tomography issues.

Indeed, the sensitivity and the resolution increase with the frequency (shorter wavelengths): a commonly adopted criterion for acoustic tests is that they can resolve defects larger than one half of the wavelength. For example, the latter resolution parameter ranges from 1000 mm for a frequency of 1 kHz to 20 mm for a frequency of 50 kHz in masonry materials characterized by a sound velocity of 2000 m/s (like the examined tuff samples), and from 2000 mm for a frequency of 1 kHz to 40 mm for a frequency of 50 kHz in more stiff masonry materials, with sound velocity of 4000 m/s.

It is worth noting that the proposed approach here does not strictly require the employ of acoustic waves in the ultrasonic range (typically from 20 kHz to 50 MHz). Indeed, the only requirement is that transducers are employed for wave generation. This allows for employing experimental tools aimed at the standardization of the amplitude of the emitted waves. On the contrary, this is not possible by employing an instrumented hammer, usual in the classical sonic tests. Notice that special transducers for longitudinal acoustic waves are available also with frequencies of 20 kHz, 10 kHz and below, in the upper bound of the sonic range (20 Hz–20 kHz).

For attenuation issues, the proposed procedure cannot be applied to thick masonry structural elements and in case of marked discontinuities (elements with large fractures and/or walls filled by a rubble masonry layer). Moreover, the stiffer is the material, the better will be the quality of the results. On the contrary, the proposed methodology appears to be very promising for relatively thin masonry elements, or to columns and pillars of stone.

The above-described features of the experimental setup open possible application fields of the proposed approach to other kinds of structures, like timber and concrete structures, not explicitly taken into consideration in this paper.

In Sect. 2, fundamentals of acoustic tomography and the underlying theoretical aspects are summarized, along with mathematical operative issues like, e.g., the inversion algorithms. In particular, in Sect. 2.1 the above concepts are specialized for the standard travel time tomography, whereas Sect. 2.2 focalizes on amplitude tomography, examining the different sources of attenuation, the modeling of the attenuation and some relevant experimental issues.

Section 3 proposes some improvements for ultrasonic amplitude tomography, aimed at overcoming the limitations for masonry structures recalled before. The combination of these improvements gives rise to the innovative approach called *Standardized Amplitude Tomography* (SAT). In particular, in Sect. 3.1 a new suitable experimental tool aimed at standardizing the emitted amplitude, regardless of the force exerted by the operator on the transducers and, to some extent, independently from the coupling conditions between the transducers and the surface of the investigated solid medium is introduced. In Sect. 3.2 a new amplitude variation model is proposed. This model represents an evolution of that in [35], taking into account also the influence of the radiation pattern of the source transducer and the receiving characteristics of the receiver. Finally, in Sect. 3.3 a strategy for avoiding initial calibrations and measurements of the emitted amplitude is proposed.

In Sect. 4 the innovative SAT approach is validated by four experimental tests on tuff samples having known internal defects like holes, cuts and inclusions. The capability of the proposed approach is discussed by the comparison with the results of the classical ultrasonic travel time tomography and of the standard amplitude tomography. This comparison highlights the effectiveness of the innovative SAT approach and suggests directions for further improvements.

2 Acoustic Tomography: Theoretical Background and Current Approaches

Mathematically speaking, tomography is a special inverse problem generalizing the Radon's problem, where the data kernel involves measurements made along rays. The Fourier Slice theorem shows how a complete slice of an object can be extracted from a proper set of measurements [42]. According to the definition in [43, 44], given a physical system and a mathematical model describing it, an inverse problem aims to infer immeasurable properties of the system (called *model parameters* if in discrete form *or model function* if in continuous form) from measurable information on the system (*observable parameters*). Clearly, observable parameters are known (data) and model parameters are unknown.

A crucial step is the definition of a mathematical model (*model equation*) relating the data with the model function (or the model parameters). In general, model equations may be nonlinear both in data and model parameters and the inverse problem may be expressed only in the implicit integral form [44]:

$$d(\mathbf{y}) = \int_a^b K(\mathbf{x}, \mathbf{y}) m(\mathbf{x}) dl, \tag{1}$$

with a and b the ends of a ray path (measurement points), $d(\mathbf{y})$ the value of the observable parameter at the point $\mathbf{y}$, $m(\mathbf{x})$ the model function at the point $\mathbf{x}$, that is, the unknown of the problem, and $K(\mathbf{x}, \mathbf{y})$ a kernel function.

In practical applications, the observable parameter is determined for a discrete number of points, resulting in a discrete set of measurements d_i, i = 1, 2, ... , N. For each of these measurements, (1) can be written:

$$d_i = \int_a^b K_i(\mathbf{x}) m(\mathbf{x}) dl. \tag{2}$$

Moreover, also the model function is usually discretized in a finite number of coefficients m_j, j = 1, 2, ... , M. Thus, once introduced a convolution N × M matrix $\mathbf{K}$ with components K_{ij} the inversion problem can be represented in the discretized form:

$$d_i = \sum_{j=1}^{M} K_{ij} m_j, \ \mathrm{i} = 1, 2, \ldots, \mathrm{N}, \tag{3}$$

or, in matrix notation:

$$\mathbf{d} = \mathbf{K}\mathbf{m}, \tag{4}$$

where $\mathbf{d}$ is a vector collecting the N measurements of the observed parameter, and $\mathbf{m}$ is a vector collecting the M unknown coefficients discretizing the model function.

From a physical point of view, the above discretization corresponds to a discretization of the domain to be investigated in M *blocks*, and therefore K_{ij} assumes the meaning of the arc length of the *i*th ray in the *j*th block [42]. In particular, in the case of 2D tomographic problems, as well as those studied in the present paper, blocks are usually called *cells* or *pixels*.

The discrete formulation (4) represents the natural data structure for discrete data values; this formulation reduces the problem to the inversion of the matrix $\mathbf{K}$ or, if $\mathbf{K}$ is noninvertible (as often happens), to the computation of a "pseudoinverse". Thus, in tomography the data inversion algorithm plays a fundamental role. Moreover, since tomography (like most inverse problems) is usually an ill-posed problem, some regularization tools shall be employed in the inversion procedure.

Many inversion algorithms have been proposed for tomographic purposes [44]: matrix inversion methods, iterative methods, etc.. The most common is the iterative algorithm called Simultaneous Iterative Reconstruction Technique (SIRT), characterized by a more stable convergence than other tomographic iterative algorithms, and capable of considering the effect of all ray-paths crossing each pixel. Anyway, in the presence of inconsistent data (and this is often the case in acoustic tomography of masonry structures) also SIRT algorithm presents some relevant convergence difficulties, and the estimated parameters could fluctuate as the iterations are progressing [44].

Among the possible tomographic NDT techniques for civil engineering structures, acoustic tomography is based on the propagation of mechanical waves, and it is used for characterizing the distribution in a cross-section of a structure of internal features like, for example, mechanical properties, discontinuities and defects. In particular, in *travel time tomography* the model parameter is the wave slowness, i.e., the inverse of wave velocity, and the observed parameter is the wave travel time. In *attenuation tomography*, instead, the model parameter is the wave attenuation coefficient, whereas the observed parameter may be the frequency of the centroid of the wave spectrum (*frequency shift method*) or the amplitude of the first peak of the received wave (*amplitude tomography*). For the reasons set out in the Introduction, in what follows the attention will be focused only on amplitude tomography.

The results of acoustic tomography may be strongly affected by modeling, experimental and mathematical issues. Indeed, it is crucial to define a suitable theoretical model relating the model parameter to the observed parameter. Experimentally, the measurements should be as precise and accurate as possible, aiming at gathering reliable data.

Mathematically, the inversion strategy must be carefully chosen.

2.1 Travel Time Tomography

Travel time tomography (TT) is by far the most used tomographic approach for concrete and masonry structures. This is due to the easiness of the experimental measurements, concerning the wave travel time from the source, placed in a given position on the perimeter of the investigated cross-section, to the receiver, placed in another position on the perimeter. The model parameter is the sectional distribution of the wave slowness $s(\mathbf{x})$; once evaluated the latter, it is possible to determine the sectional distribution of the wave velocity, which is represented in the tomographic map.

Wave velocity is strictly related to physical and mechanical properties like, e.g., the density and the elastic constants; moreover, if there are cracks or voids, wave travel time increases, and this yields to an apparent reduction of wave velocity. Thus, the tomographic map immediately gives a representative overview of the internal features of the solid medium, relevant for structural analysis purposes.

In TT, the model equation relating the travel time with the slowness is usually determined according to the following two hypotheses. First, the ray theory is considered for modelling wave propagation. Ray theory is based on a high-frequency approximation of the solution of the elastodynamic problem for a generally heterogeneous solid medium [45]; this approximation is plausible only for high frequency waves or, equivalently, for smoothly varying media with respect to the wavelength. Second, it is assumed that the solid under investigation is a non-dispersive medium, and therefore that wave velocity does not depend on wave frequency.

By the above two hypotheses, in the i*th* measurement for an arbitrary ray path $\wp$ connecting the source and the receiver the travel time $t_{\wp}$ can be expressed as [46]:

$$t_{\wp} = \int_{\wp} s(\mathbf{x}) dl, \tag{5}$$

where the line integral is performed along the ray path $\wp$. The *Fermat's principle* allows for identifying, among the infinite possible, the actual ray path $\mathfrak{R}_i$, that is, the ray path of least overall travel time, minimizing (5) with respect to all possible ray paths $\wp$ [46]:

$$t_i = \int_{\mathfrak{R}_i} s(\mathbf{x}) dl = \min_{\wp} \int_{\wp} s(\mathbf{x}) dl, \tag{6}$$

with t_i the actual travel time. For tomographic purposes, the actual ray path $\mathfrak{R}_i$ is determined by ray-tracing algorithms, see, e.g., [47].

Therefore, the discretized form (3) of the travel time tomographic problem becomes:

$$t_i = \sum_{j=1}^{M} L_{ij} m_j, \ \mathrm{i} = 1, 2, \ldots, \mathrm{N}, \tag{7}$$

or, in matrix notation:

$$\mathbf{t} = \mathbf{L}\mathbf{m} \tag{8}$$

where the components L_{ij} of the $\mathrm{N} \times \mathrm{M}$ matrix $\mathbf{L}$ represent the arc length of the *i*th ray in the *j*th pixel, $\mathbf{t}$ is a vector collecting the N measurements of the travel time (observed parameter), and $\mathbf{m}$ is a vector collecting the M unknown slowness coefficients (model parameters).

2.2 Amplitude Tomography

Amplitude tomography (AT) aims at evaluating the distribution $a(\mathbf{x})$ of the wave material attenuation coefficient (model parameter) in a cross-section of the investigated solid medium starting from the measurement of the decrease of the wave first peak amplitude from the source to the receiver (observed parameter).

It is worth noting that when an acoustic wave propagates through a solid medium, its amplitude reduces for two primary attenuation phenomena: a) material attenuation and b) geometrical attenuation. Other sources of attenuation might be: c) reflection, refraction and mode conversion at interfaces; d) wave dispersion (both velocity and attenuation dispersion); e) scattering and diffraction due to obstacles and voids; f) multipath phenomena; g) the radiation pattern of the source probe; h) the receiving characteristic of the receiver (the receiving pattern for PZT transducers, or the normal and tangential sensitivity with respect to the surface of the transducer if the receiver is an accelerometer) [48, 49]. To be representative, a comprehensive amplitude variation model, relating the attenuation coefficient to the measured amplitude decrease, should consider all the above-listed attenuation sources.

In current AT approaches – from here on called *ordinary amplitude tomography* (OAT) in order to distinguish them from the innovative AT approach here proposed – generally only a few of the above-listed attenuation sources are taken into account, and in particular only material and geometrical attenuation. In so doing, according to [35] in the *i*th measurement, for the generic ray path $\wp$ connecting the source and receiver it is possible to write:

$$A_i = B_0 g\left(l_{\wp}\right) e^{-\int_{\wp} a(\mathbf{x}) dl}, \tag{9}$$

with A_i the first peak wave amplitude measured at the receiver, B_0 the first peak amplitude of the emitted wave, $l_{\wp}$ the length of the ray path $\wp$ and $g\left(l_{\wp}\right)$ the value assumed by

the geometrical attenuation $g(l)$ at the end of the ray path $\wp$, i.e., at the receiver.

As in TT, it is possible to determine the actual ray path $\mathfrak{R}_i$ by a ray-tracing algorithm, see e.g.[31]. This way, the model equation assumes the following expression:

$$A_i = B_0 g\left(l_{\mathfrak{R}_i}\right) e^{-\int_{\mathfrak{R}_i} a(\mathbf{x})dl}. \tag{10}$$

According to [35], it is possible to take $g(l) = (1/l)^{\beta}$, with $\beta = 0.5$ for cylindrical wavefronts and $\beta = 1.0$ for spherical wavefronts, and $B_0 = A_0\left(l_0\right)^{\beta}$, with A_0 the amplitude measured at an arbitrary distance l_0. Therefore, (10) yields:

$$A_i = A_0\left(\frac{l_0}{l_{\mathfrak{R}_i}}\right)^{\beta} e^{-\int_{\mathfrak{R}_i} a(\mathbf{x})dl}. \tag{11}$$

In order to get a form useful for tomographic applications, (11) can be manipulated as follows:

$$\ln\left[\frac{A_0}{A_i}\left(\frac{l_0}{l_{\mathfrak{R}_i}}\right)^{\beta}\right] = \int_{\mathfrak{R}_i} a(\mathbf{x})dl. \tag{12}$$

Now, by reducing the model function $a(\mathbf{x})$ to M model parameters describing the material attenuation a_j, j = 1, 2, ..., M (a_j is the material attenuation coefficient at the pixel j), and by putting:

$$g_i = \ln\left[\frac{A_0}{A_i}\left(\frac{l_0}{\sum_{j=1}^{M} L_{ij}}\right)^{\beta}\right],\ \mathrm{i} = 1, 2, \ldots, \mathrm{N}, \tag{13}$$

(12) can be discretized in a model equation of the form (3):

$$g_i = \sum_{j=1}^{M} L_{ij} a_j,\ \mathrm{i} = 1, 2, \ldots, \mathrm{N}. \tag{14}$$

The data g_i for the ith measurement has to be calculated starting from the measured value of the first peak wave amplitude A_i; notice that (13) contains two parameters: A_0, the amplitude measured at the arbitrary distance l_0, and l_0 itself.

In matrix notation, (14) may be written as:

$$\mathbf{g} = \mathbf{La}, \tag{15}$$

where the meaning of the symbols is clear from the above.

In AT, some relevant experimental problems arise. Indeed, some technical issues can affect the reliability of wave amplitude measurements at the receiver: the coupling conditions between the probes and the surface of the investigated solid medium, that are usually unknown and may vary in an unpredictable way due to the thinning of the coupling medium, or to the variation of the pressure exerted by the operator on the transducers (in terms of magnitude and distribution), or to the variation of features like the roughness of the investigated surfaces. Moreover, again for the uncertainties of coupling conditions, it is difficult to evaluate the amplitude of the emitted wave, corresponding to B_0 in (10), as well as the amplitude A_0 at the arbitrary distance l_0 in (13).

The influence of the above experimental issue in the accuracy of AT results is usually underestimated; indeed, it is common to employ the same experimental setup used for TT. However, travel time can be measured in a much more reliable way than the amplitude, strongly affected by the coupling conditions. Then, often the quality of the results obtained by AT on civil structures is very poor, and this strongly obstructs the use of AT approaches.

3 Proposed Improvements of AT: Standardized Amplitude Tomography

In order to overcome some of the limitations of OAT approaches for civil structures, in this paper a novel approach to amplitude tomography, called *Standardized Amplitude Tomography* (SAT), is proposed. The improvements concern two fundamental issues of amplitude tomography: the experimental setup and the model equation. Moreover, an alternative approach for evaluating the parameter B_0 in (10), representing the first peak amplitude of the emitted wave, is adopted.

SAT is thought for applications to masonry constructions and, indeed, this new approach is validated through experimental tests on masonry specimens. However, SAT approach can be applied to timber and concrete constructions as well, although in the latter applicative field the resolution achievable with standard travel time ultrasonic tomography is much more satisfactory.

3.1 Improvements of the Experimental Setup

As recalled just above, possible variations of the coupling conditions could drastically affect the value of the amplitude measured at the receiver: this observation suggested the development of a specific experimental setup aimed at minimizing the uncertainties in the amplitude data due to the variation of the coupling conditions.

Based on the experimental results reported in Appendix, showing a marked correlation between the force pulling the transducers and the measured amplitude, an experimental tool aimed at leveling the pressure of the transducers on the investigated surface, regardless of the pressure exerted by the operator during the tomographic test, has been designed and built (see Fig. 1). Basically, this tool consists of a sleeve

Fig. 1 Experimental tool aimed at leveling the pressure on the transducers

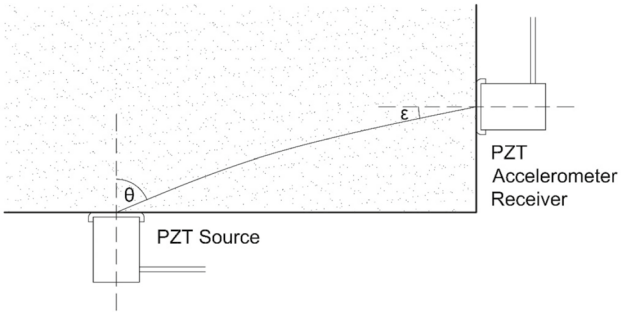

Fig. 2 Spatial angles of the source and the receiver

housing the transducer, with a spring placed between the handle for the operator and the transducer. The spring and the stroke of the transducer in the sleeve have been designed in order to apply a nearly constant force of about 50 N on the transducer when the instrument is pushed against the measurement surface.

At our knowledge, a similar functional principle has been already employed in advanced arrays of ultrasonic probes for tomographic inspection of concrete structures. However, the special handle is proposed here to manage big low-frequency ultrasonic probes and has the peculiarities of being expressly designed for leveling the pressure in order to improve amplitude measurements, and of being very simple and inexpensive to manufacture. The application of this device is for tomographic inspection either of masonry structures (like in case of the present paper), or of concrete structures.

If this special handle is used for operating both the source and the receiver, and if the surface of the investigated solid has uniform physical and mechanical properties (impedance, roughness, etc.), the coupling conditions can be considered substantially invariant during the test, and consequently the amplitude of the emitted and received waves is rather independent from the pressure exerted by the operator, as it is discussed in Appendix. This justifies the adjective "*Standardized*" in the name given to the innovative approach proposed in the present paper.

3.2 Improvements of the Amplitude Variation Model

In Sect. 2.2 it is underlined that OAT model equations like (10) consider only some of the sources of wave amplitude attenuation. In view of developing effective amplitude tomography procedures for application to civil structures, in this paper the model equation is improved taking into account also the influence of the radiation pattern of the source transducer and the receiving characteristic of the receiver transducer.

Indeed, it is well known that given a propagation medium, at a fixed distance from the center of a source transducer, the spatial distribution of the generated acoustic pressure depends also from the direction. This dependence is described by a radiation pattern. Similarly, the sensitivity of a receiver transducer depends also on the direction according to a receiving pattern. In particular, a PZT receiver is characterized by a receiving pattern having the same directional features of the radiation pattern of source transducers, whereas when the receiver is an accelerometer generally only the component of the wave displacement field orthogonal to the surface of the transducer is detected. In conclusion, it follows that the measured value of the received wave amplitude is strongly influenced by the direction.

Here, the directivity features of the radiation pattern of the source transducer are represented by a function $d(\theta)$, where θ is the spatial angle from the axis of the source, and the directivity aspects of the receiver are represented by a function $r(\varepsilon)$, where ε is the spatial angle from the axis of the receiver (see Fig. 2). Accordingly, (10) is modified in:

$$A_i = B_0 g\left(l_{\Re_i}\right) d\left(\theta_i\right) r\left(\varepsilon_i\right) e^{-\int_{\Re_i} a(\mathbf{x}) dl}, \tag{16}$$

where the spatial angles θ and ε are referred to the ith measurement. Now, since by [35] it is possible to assume $g(l) = (1/l)^{\beta}$ (see Sect. 2.2), it results:

$$A_i = \frac{1}{\left(l_{\Re_i}\right)^{\beta}} B_0 d\left(\theta_i\right) r\left(\varepsilon_i\right) e^{-\int_{\Re_i} a(\mathbf{x}) dl}. \tag{17}$$

The latter equation can be expressed in a format suitable for tomographic applications as follows:

$$\ln\left[\frac{B_0}{A_i} \frac{d\left(\theta_i\right) r\left(\varepsilon_i\right)}{\left(l_{\Re_i}\right)^{\beta}}\right] = \int_{\Re_i} a(\mathbf{x}) dl. \tag{18}$$

Now, by putting:

$$g_i = \ln\left[\frac{B_0}{A_i}\frac{d(\theta_i)r(\varepsilon_i)}{\left(\sum_{j=1}^{M} L_{ij}\right)^{\beta}}\right],\ \mathrm{i} = 1, 2, \ldots, \mathrm{N}, \tag{19}$$

(18) can be discretized in the form (14), or in matrix notation in the form (15).

In principle, the functions $d(\theta)$ and $r(\varepsilon)$, appearing in the above equations, should be determined through experimental tests: indeed, their expressions depend on the characteristics of the transducers and of the investigated solid medium, and therefore usually both are unknown in advance.

In order to render the proposed approach feasible, the strategy here proposed is that of adopting for $d(\theta)$ and $r(\varepsilon)$ the simplest analytical expressions available in the literature, i.e., the expressions for cylindrical transducers in the so-called acoustic case [45, 49]. Notice that the latter expressions refer to wave propagating in fluid media; anyway, they allow for taking into account the influence of the direction on the measured wave amplitude value, although in a very simplified way. This already ensures a substantial improvement in the accuracy of tomographic results.

In particular, with respect to the source directivity function $d(\theta)$, for a cylindrical source transducer and for the acoustic case, in the far field (the Fraunhofer region) it is possible to assume [49, 50]:

$$d(\theta) = \frac{2J_1(kR\sin\theta)}{kR\sin\theta}, \tag{20}$$

where J_1 is the Bessel function of the first kind of order one, R is the radius of the transducer surface, $k = \omega/v$ is the wavenumber of the emitted wave, with angular frequency ω and velocity v. Notice that both ω and v are not known in advance. Therefore, with respect to the wave velocity v the mean value of the wave velocity distribution $v(\mathbf{x})$ obtained by a preliminary travel time tomography, needed also for determining the actual ray paths, has been considered in the proposed approach. Specifically, by adopting a homogeneous pixel discretization the mean value of $v(\mathbf{x})$ can be computed as the arithmetic mean value of the local wave velocity v_j determined for each pixel. Moreover, with respect to the evaluation of the angular frequency ω, it should be pointed out that (20) rigorously holds for continuous waves, whereas transducers usually emit pulses. To overcome this issue, according to the considerations in [49] narrowband transducers have been used and ω has been identified with the peak frequency of the emitted wave.

Regarding the receiver directivity function $r(\varepsilon)$, for PZT receivers the reciprocity theorem [51] states that the receiving pattern has the same directional features of the radiation pattern of source transducers; thus, it is possible to assume:

$$r(\varepsilon) = \frac{2J_1(kR\sin\varepsilon)}{kR\sin\varepsilon}, \tag{21}$$

where the symbols have the same meaning of those in (20); furthermore, the same observations about the determination of the angular frequency and the wave velocity hold.

With respect to accelerometric receivers, $r(\varepsilon)$ depends on the sensitivity of the transducer in directions normal and tangential (three mutually orthogonal directions) with respect to its surface. The most common case is that of accelerometers sensitive only in the direction of their axis, that is, capable of measuring only the component of the amplitude orthogonal to the surface of the transducer. For this special case, by simple geometric considerations suggested by Fig. 2, it is possible to take:

$$r(\varepsilon) = \cos\varepsilon. \tag{22}$$

3.3 Evaluation of the Parameter B_0

By (14) and (18) the discretized model equation can be written in the form:

$$\ln\left[\frac{B_0}{A_i}\frac{d(\theta_i)r(\varepsilon_i)}{\left(\sum_{j=1}^{M} L_{ij}\right)^{\beta}}\right] = \sum_{j=1}^{M} L_{ij}a_j, \tag{23}$$

where, besides the unknown material attenuation coefficients a_j all the terms have to be considered known or measured, except for B_0, representing the first peak amplitude of the emitted wave.

As it is recalled in Sect. 2.2, for the OAT formulation in [35] it is assumed that $B_0 = A_0(l_0)^{\beta}$, where A_0 is the first peak amplitude measured at an arbitrary distance l_0, to be determined by a calibration procedure. Anyway, when the internal features of the investigated structure are unknown, as in the cases of our interest, this calibration becomes practically unreliable, causing possible large errors in the evaluation of B_0.

For this reason, here a different strategy for determining the parameter B_0 is proposed. In particular, since the data gathered (i.e., the measured values of the observed parameter) are usually largely redundant, thus making the tomographic equations form a highly overdetermined system, it is possible to include B_0 among the unknowns to be determined by the inversion of the tomographic equations. A

similar approach is adopted in [31] with reference to another unknown tomographic parameter.

From a mathematical point of view, (23) can be arranged in the form:

$$\ln B_0 + \ln\left[\frac{1}{A_i}\frac{d(\theta_i)r(\varepsilon_i)}{\left(\sum_{j=1}^{M} L_{ij}\right)^{\beta}}\right] = \sum_{j=1}^{M} L_{ij}a_j; \tag{24}$$

then, if a test value $\tilde{B}_0$ for the unknown parameter B_0 is considered, the factor:

$$q = \ln \tilde{B}_0 - \ln B_0 \tag{25}$$

can be introduced; notice that q in (25) is unknown, since B_0 is. By adding (25) to both sides of (24), it follows:

$$\ln \tilde{B}_0 + \ln\left[\frac{1}{A_i}\frac{d(\theta_i)r(\varepsilon_i)}{\left(\sum_{j=1}^{M} L_{ij}\right)^{\beta}}\right] = \sum_{j=1}^{M} L_{ij}a_j + q, \tag{26}$$

that can be written in the classic tomographic form:

$$\tilde{g}_i = \sum_{j=1}^{M+1} H_{ij}h_j, \tag{27}$$

where:

$$\tilde{g}_i = \ln\left[\frac{\tilde{B}_0}{A_i}\frac{d(\theta_i)r(\varepsilon_i)}{\left(\sum_{j=1}^{M} L_{ij}\right)^{\beta}}\right], \tag{28}$$

H_{ij} are the components of a N × (M + 1) matrix **H** obtained from the N × M matrix **L** by adding a last column whose components are all equal to 1, and h_j are the M + 1 components of a vector **h** having the first M components equal to those of the vector **a**, and the last component equal to q in (25). Equation (27) can be represented in matrix notation as:

$$\tilde{\mathbf{g}} = \mathbf{Hh}. \tag{29}$$

Notice that the transformation of (26) in (27) has not only a formal meaning because it corresponds to the choice of including q among the unknown of the tomographic problem in addition to the attenuation coefficients a_j.

The linear system (29) can be inverted by using a classical tomographic approach, obtaining as the solution the vector **h**, and therefore the vector of the unknown attenuation coefficients **a** and the value of the factor q. This way, the unknowns in **a** are determined with reference to the correct value of B_0, that is:

$$B_0 = \frac{\tilde{B}_0}{e^q}. \tag{30}$$

In the implementation of the above algorithm for evaluating B_0 is recommended to perform some iterations for enhancing the precision of the results. For each iteration, the value of B_0 determined at the end of the previous iteration should be taken as the test value $\tilde{B}_0$. The iterations can be stopped when no significant variations in the values of B_0 are observed.

The described strategy for evaluating B_0 is very effective and robust if the number of data gathered is largely redundant and if the coupling conditions can be considered substantially invariant during the test. Clearly, for the validity of the latter condition the use of experimental devices like that described in Sect. 3.1 and the uniformity of physical and mechanical properties of the investigated surfaces (impedance, roughness, etc.) are needed.

4 Experimental Validation and Discussion

For the validation of the proposed innovative Standardized Amplitude Tomography (SAT) procedure, an experimental campaign has been carried out.

In the experiments, 4 different specimens have been analyzed (Test 1, 2, 3 and 4) by SAT; moreover, to evaluate the effectiveness of SAT with respect to ordinary TT and OAT, also the latter procedures have been applied. All specimens included known internal defects specifically designed simulating real-life defects as cracks, voids and inclusions, and for stressing the limitations of the tomographic procedures under investigation. All the specimens were in Apulian tuff, a material widely employed for historic masonry constructions of Apulia, in Italy.

The experimental setup consisted of a commercial apparatus for sonic and ultrasonic tests on masonry and concrete, called Boviar Solgeo CMS. An ultrasonic PZT probe (TSG-55) with a nominal frequency of 55 kHz has been used as the source transducer, and an active high sensitivity PZT accelerometer (RSG-55) has been used as the receiver transducer. The control unit was equipped with a 12-bit data acquisition card, capable of acquiring signals with frequencies between 50 kHz and 1,25 MHz. A time/amplitude window, with the time displayed in μs and the amplitude in mV, allowed for

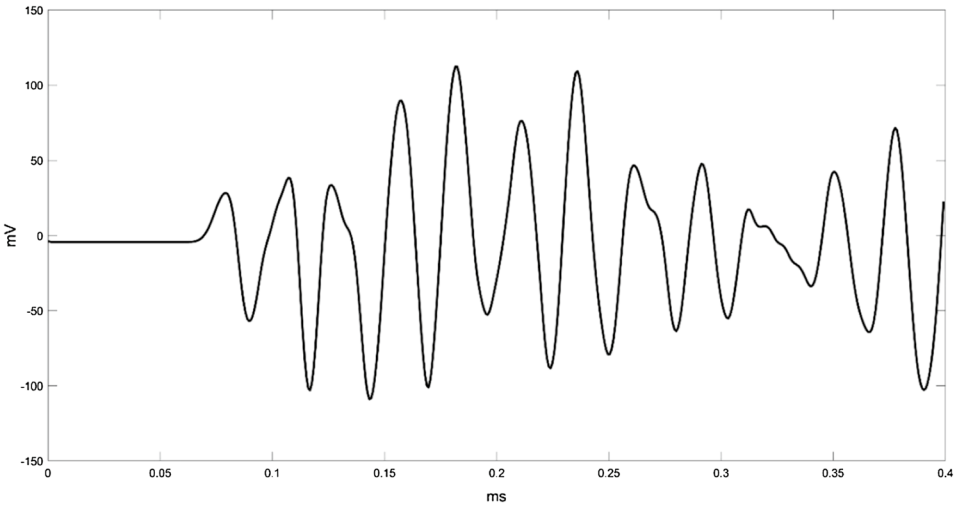

Fig. 3 Sample of the received signals

visualizing the acquired signals. A sample of a received signal is contained in Fig. 3.

For both the source and the receiver transducers plasticine has been used as the coupling medium to tuff specimens. Moreover, during all the tests, both the source and the receiver transducers have been handled by the experimental tool described in Sect. 3.1; this allows for pushing the transducers against the specimen surface with a practically constant force of 50 N. Finally, in all the performed tests source and receiver transducers were always placed on opposite or neighboring sides of the specimen, and thus no measurements have been made with the transducers on the same side of the specimen.

The experiments have been performed in normal ambient conditions; the mass density of the examined tuff was of about 1400 kg/m^3.

With respect to travel time evaluations, for each measurement path three ultrasonic pulses were emitted and for each of them the received signal was acquired and normalized with respect to the maximum waveform amplitude. Then, a threshold of 5% of the maximum normalized amplitude was set for the determination of the first peak, such that all the peaks below the threshold are considered as noise. The time of flight (TOF) of each ultrasonic pulse is then selected to be the first time point where the signal is above the threshold level. Finally, for the considered measurement path the average of the three TOF values determined according to the above has been identified as the travel time.

With respect to amplitude evaluations, the amplitude of the first peak above the considered threshold has been taken. This approach, according to [29], yields a more consistent data set. In particular, the amplitude for the considered measurement path has been determined as the average of the actual amplitudes of the first peak (above the threshold) of the three signals.

For data processing, some ad hoc MATLAB™ scripts have been created, and for tomographic inversion the commercial software aTom™ by Adding Ltd. and Solgeo Ltd. has been used. The latter performs the reconstruction of the wave paths (ray-tracing) and then iteratively determine the distribution of the model parameters (ultrasound velocity or attenuation) by the SIRT inversion algorithm.

In what follows the results obtained in the above-mentioned experimental campaign are described. The reconstruction of the internal features of each specimen obtained by SAT, TT and OAT has been discussed in order to assess the capability of the three different tomographic approaches to detect defects and to give a reliable map of the internal morphology.

In particular, the tomographic maps in figures represent the distribution in the cross-section of the specimen of the ultrasound velocity (m/s) for TT, and of the attenuation (1/m) for OAT and SAT. In what follows, the color scales of tomographic maps are arranged in such a way as to enhance to the greatest possible extent the resolution with respect to internal inhomogeneities. In other words, the minimum and the maximum value of the ultrasound velocity or of the attenuation are chosen such that the observer get the best perception of the inhomogeneity in the distribution of the model parameters. Moreover, the tomographic maps contain an outline of the defects for an immediate qualitative assessment.

Finally, it is worth noting that both amplitude tomography maps, OAT maps and SAT maps, are obtained starting from the same data on the amplitude of the received signals. Thus, the improvements of SAT over OAT in terms of the resolution are exclusively due to the enhancements of the model equation described in Sect. 3.2–3.3.

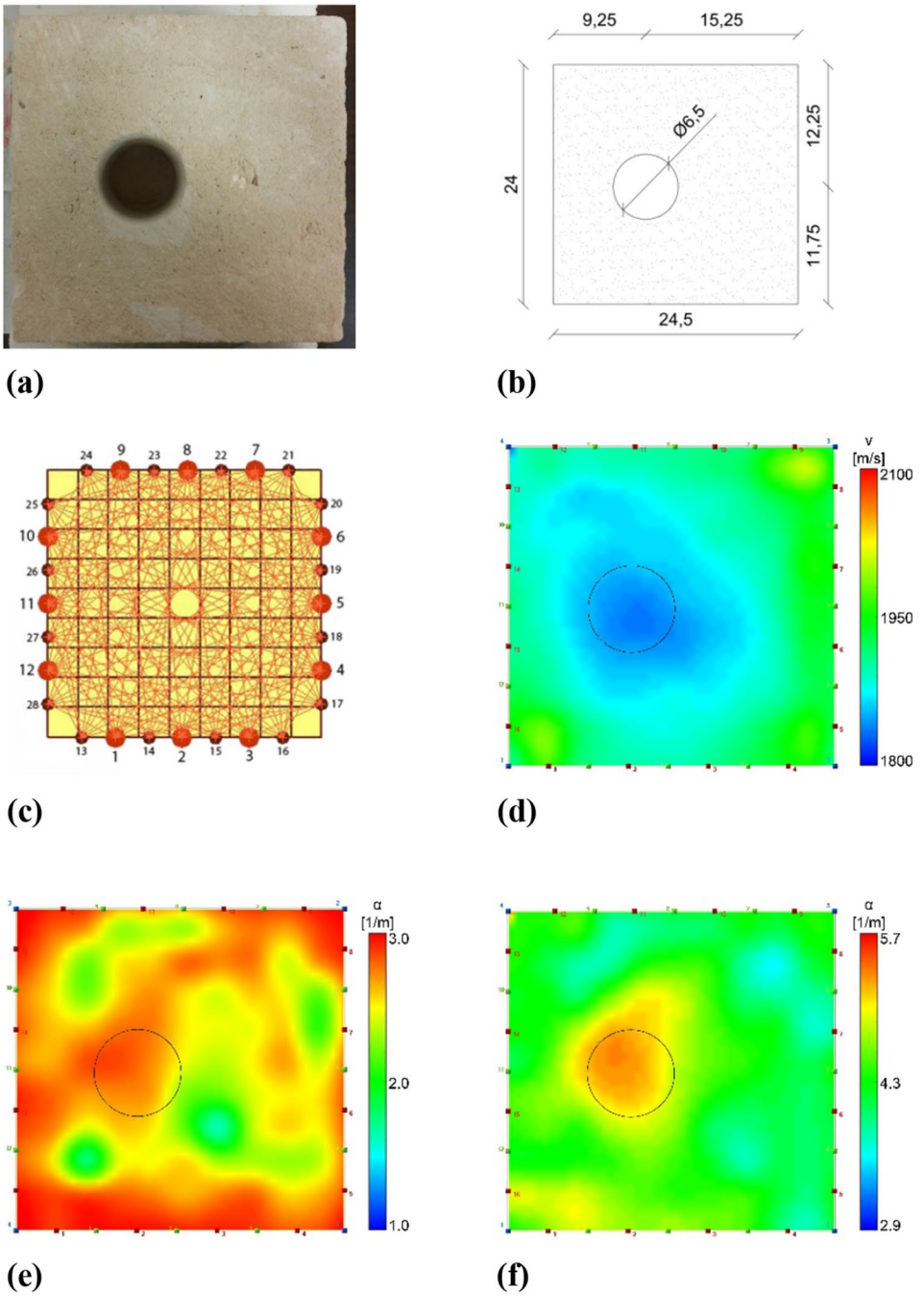

Fig. 4 **a** Picture of the specimen. **b** Relevant dimensions of the specimen and of the defect (cm). **c** Layout of tomographic measurements. **d** TT velocity map (m/s). **e** OAT attenuation map (1/m). **f** SAT attenuation map (1/m)

4.1 Test 1

Test 1 concerned a cubic tuff block with a cross-section of 24.5 cm × 24.0 cm, with a drilled pass-through hole having 6.5 cm diameter (see Fig. 4a, b). The study of this specimen aims at assessing the sensitivity of the tomographic techniques under investigation in detecting a big defect (a big void) with a very marked discontinuity in the acoustic impedance. For the tomography, 144 measurements were carried out; the mutual position of the source and the receiver transducers are displayed in Fig. 4c, that also shows the discretization of the cross-section in $9 \times 9 = 81$ pixels.

The obtained results are displayed in Figs. 4d (velocity map obtained by standard TT procedure), 4e (attenuation map obtained by standard OAT procedure) and 4f (attenuation map obtained by the innovative SAT procedure).

Firstly it emerges that, despite the use of the experimental tools aimed at leveling the pressure of the transducers on the specimen (anyhow improving the quality of the results),

the standard amplitude tomographic approach (OAT) gives back a tomographic map (Fig. 4e) completely inconsistent with the actual internal morphology of the specimen. This result justifies why amplitude tomography is almost never employed for analyzing masonry structures.

Both the maps obtained by the standard travel time tomography (Fig. 4d) and SAT (Fig. 4f) reveal the presence of a pseudo-circular damaged area, but comparing the results it is clear that SAT gives back a sharper image of the actual internal morphology of the specimen, allowing for a much more accurate determination of the location and of the dimensions of the defect.

Anyway, both TT and SAT maps exhibit some inconsistencies; in particular, TT map (Fig. 4d) presents a little low-velocity area top right, which does not correspond to any discontinuity of the specimen, and SAT map presents a little wider high attenuation area low left, also not related to visible discontinuities of the specimen.

It is possible to conclude that for the examined specimen having a relatively large pass-through hole, SAT not only is validated by the experiments, but also can be considered the more effective technique among those considered. In particular, SAT results are more accurate than TT results. This result is arguably ascribable to the well-known limitation of TT in reconstructing the exact shape and extension of low-velocity anomalies, like the examined hole. Indeed, these anomalies determine a deviation of acoustic rays with a relatively small change in the distance traveled, and then of the travel-time in the solid domain; therefore in TT these kinds of defect result in a smooth and far from the real velocity reduction, distributed in an area quite larger of the actual defect dimension.

4.2 Test 2

Test 2 concerned the same cubic tuff block considered in Test 1 (see Sect. 4.1), examined again after the pass-through hole has been filled with a mortar having approximately the same acoustic impedance of the tuff block material (Fig. 5a, b). Now, the aim of the test is that of assessing if the tomographic techniques under investigation can characterize discontinuities in the material without the presence of cracks or voids, and without marked differences in the acoustic impedance. Also in this case, 144 measurements were carried out for the tomography, as it is represented in Fig. 5c, that also shows the discretization of the cross-section in $9 \times 9 = 81$ pixels.

The obtained results are displayed in Figs. 5d (velocity map obtained by standard TT procedure), 5e (attenuation map obtained by standard OAT procedure) and 5f (attenuation map obtained by the innovative SAT procedure).

For the standard amplitude tomographic approach (OAT) the same comments made for Test 1 hold: the obtained tomographic map is meaningless and is incapable of describing the actual internal morphology of the specimen (see Fig. 5e).

On the contrary, TT and SAT provide more appreciable results. Specifically, differently from what observed about Test 1, now TT map (Fig. 4d) characterizes the anomaly (the filled hole) more accurately than SAT map (Fig. 5f). A possible explanation of the difference between Test 1 and Test 2 results is that in Test 2 the anomaly and the rest of the tuff block have similar acoustic impedance, and then the wave energy reflected by the hole is very small, especially if compared with what is reasonable to expect in Test 1. In synthesis, the obtained results suggest that when the discontinuity is represented by the coexistence of different materials divided by an interface, travel time appears to be a more reliable parameter, whereas in presence of voids or cracks the attenuation allows for a better reconstruction of the internal morphology.

It is worth noting that also in Test 2 the TT map is quite blurred and presents a little low-velocity area top right not corresponding to visible discontinuities of the specimen. SAT map shows a high attenuation area actually corresponding to the filled hole, but presents also a higher attenuation area low left with no physical meanings, and wrongly suggests the presence of a discontinuity top left.

In conclusion, Test 2 validates SAT, but in this case TT reveals to be more effective. Moreover, the comparison of the results of Test 1 and Test 2 indicates that TT and SAT are capable of better detecting different kind of defects, and then that for a better reconstruction of the internal morphology of the masonry it could be convenient to carry out both TT and SAT tomographic analyses.

4.3 Test 3

The specimen employed for Test 3 was a prismatic tuff block with cross-section dimensions 48.5 cm × 24.5 cm (Fig. 6a, b), presenting three artificial defects: two pass-through holes, one with diameter 4.5 cm (top left) and one with diameter 2.5 cm (bottom right), and a cut that runs through the whole thickness of the block and has the depth of about 8.0 cm (bottom center).

The aim of the test is that of assessing if the tomographic techniques under investigation can detect and distinguish different and well-separated kind of defects simultaneously present in the specimen. In this case, tomography is based on 236 measurements, whose layout is depicted in Fig. 6c, that also shows the discretization of the cross-section in $9 \times 18 = 162$ pixels.

The obtained results are displayed in Figs. 6d (velocity map obtained by standard TT procedure), 6e (attenuation map obtained by standard OAT procedure) and 6f (attenuation map obtained by the innovative SAT procedure).

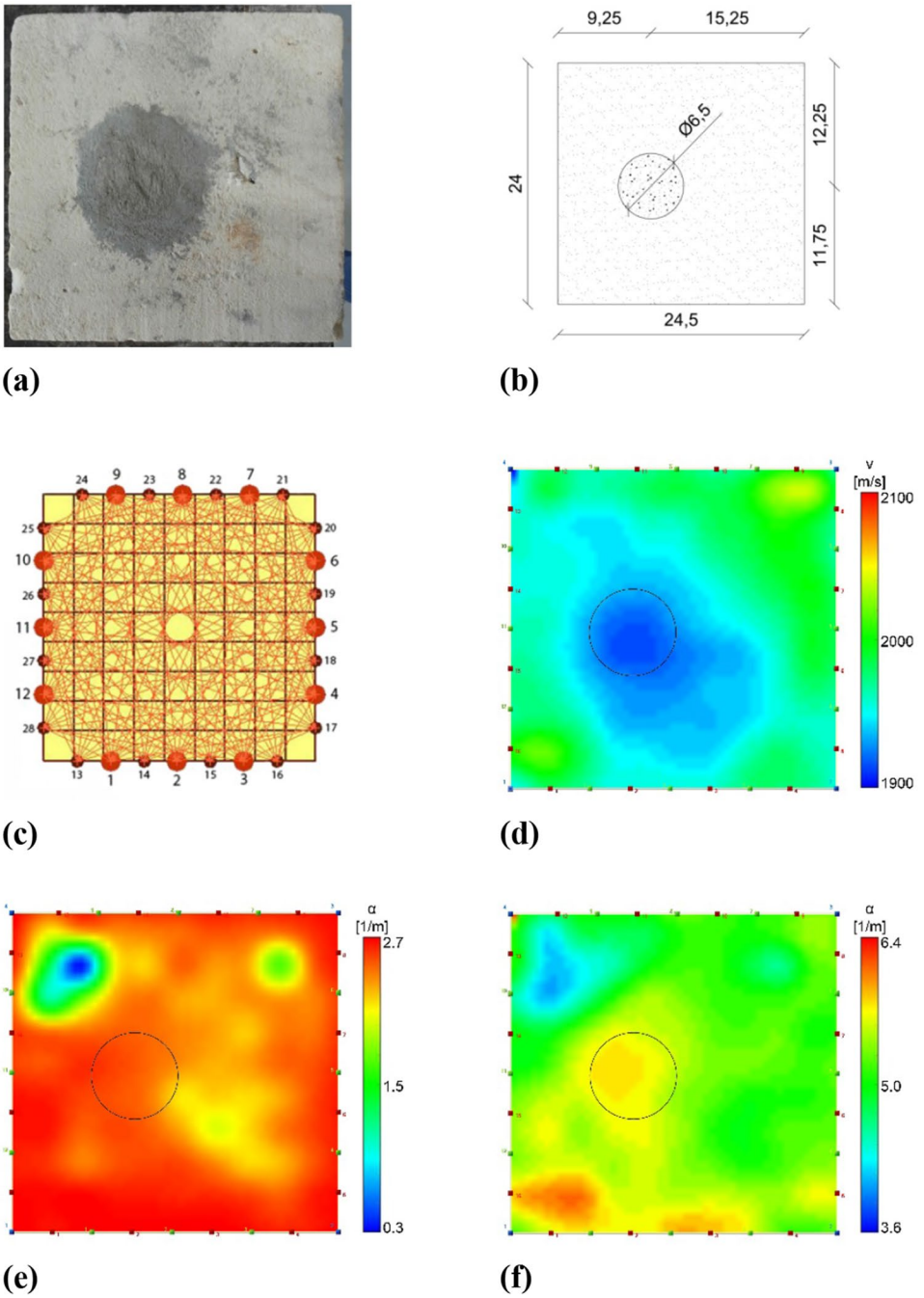

Fig. 5 **a** Picture of the specimen. **b** Relevant dimensions of the specimen and of the defect (cm). **c** Layout of tomographic measurements. **d** TT velocity map (m/s). **e** OAT attenuation map (1/m). **f** SAT attenuation map (1/m)

Test 3 confirms the total failure of OAT in understanding the internal features of the examined specimen (Fig. 6e). But, in this case, also TT and SAT give results of quite low quality. Indeed, Fig. 6d shows that TT map indicates the presence of a low-velocity area near the cut edge of the specimen, but the low-velocity area has a shape very different from that of the actual defect, being parallel to the bottom edge and not, instead, orthogonal. Moreover, a less defined and smaller low-velocity area is detected near the actual position of the smaller hole, but at some distance. The larger hole is not detected at all. Finally, the map determined by SAT (Fig. 6f) presents a high attenuation area near the cut (also in this case the area indicating the defect is parallel to the bottom edge rather than orthogonal) and near the larger hole; furthermore, a marked high attenuation area is detected below the smaller hole, and another high attenuation area is found in correspondence of the bigger hole (top left).

It is worth noting that the area of holes of Test 3 is quite smaller than the area of the defect of Test 1; in particular, in

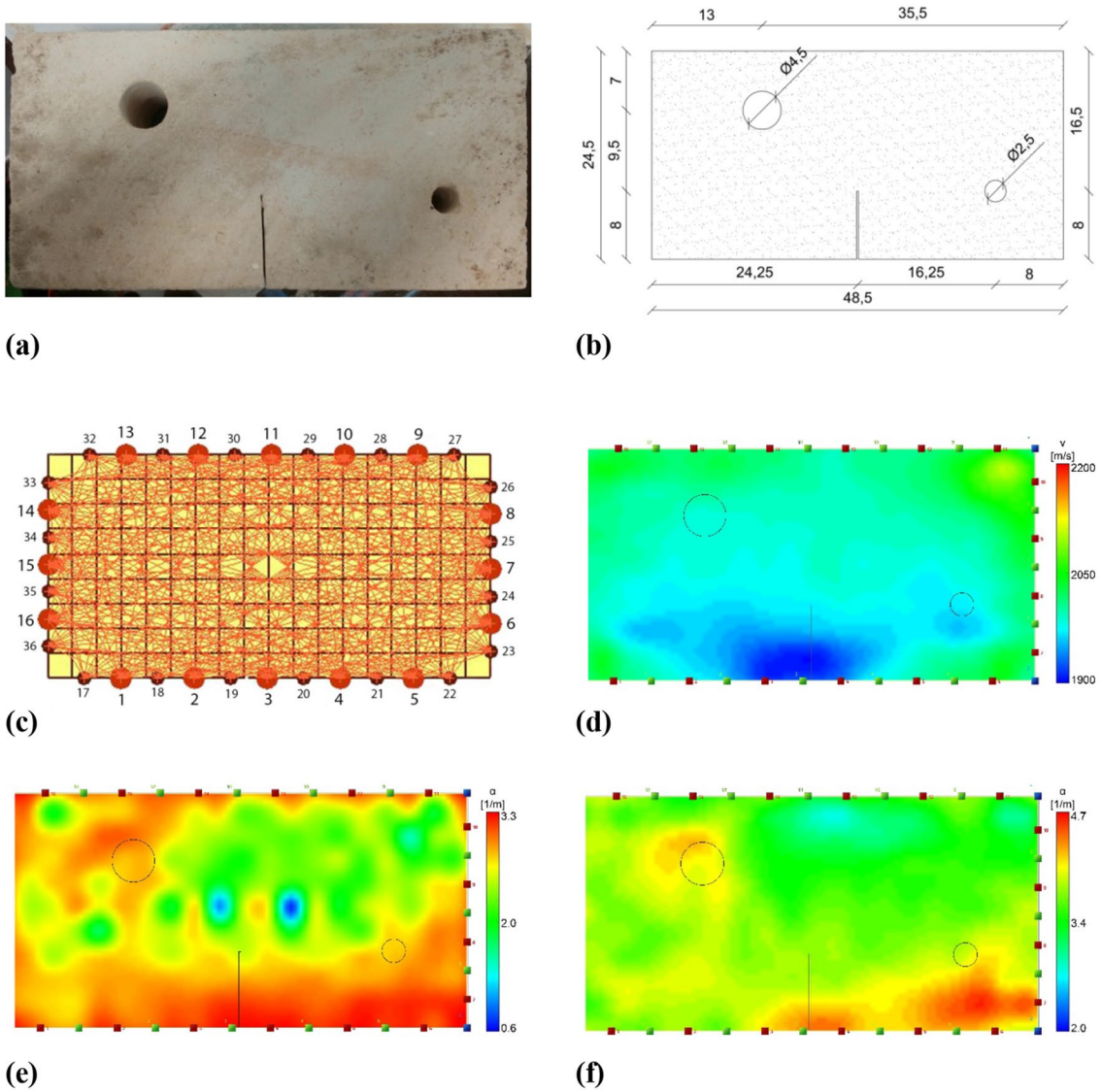

Fig. 6 **a** Picture of the specimen. **b** Relevant dimensions of the specimen and of the defects (cm). **c** Layout of tomographic measurements. **d** TT velocity map (m/s). **e** OAT attenuation map (1/m). **f** SAT attenuation map (1/m)

Test 3 the area of the holes is around 48% (the larger) and 11,5% (the smaller) of the area of the hole considered in Test 1: this could partially justify the difficulties of TT and SAT approach in detecting the defects of the specimen in Test 3, albeit in Test 1 both techniques give quite satisfactory results. Indeed, the observed difference between Test 3 and Test 1 may be ascribable to the wavelength. Indeed, for the employed frequency of 50 kHz and for ultrasound velocities around 2000 m/s the wavelength turned out to be around 4 cm. A classic criterium in ultrasonic tests is that a discontinuity must be larger than one-half the wavelength to stand a reasonable chance of being detected. Now, in Test 1 the diameter of the hole is larger than the wavelength, whereas in Test 3 the diameter of the hole is (intentionally) similar or smaller than the wavelength, and this is very challenging for the detection.

In conclusion, it is possible to claim that TT does not allow for identifying the big hole, but detects (although badly) the cut and the small hole; SAT allows for a quite rough characterization of the actual position and dimension of the holes (with worst and somewhat misleading results for the smaller hole) and of the cut. Moreover, also the results of Test 3 suggest that the detection capability of TT and SAT are to some extent complementary.

4.4 Test 4

In Test 4 another prismatic tuff specimen with a cross-section of dimensions 48.5 cm × 24.5 cm was analyzed (Fig. 7a,

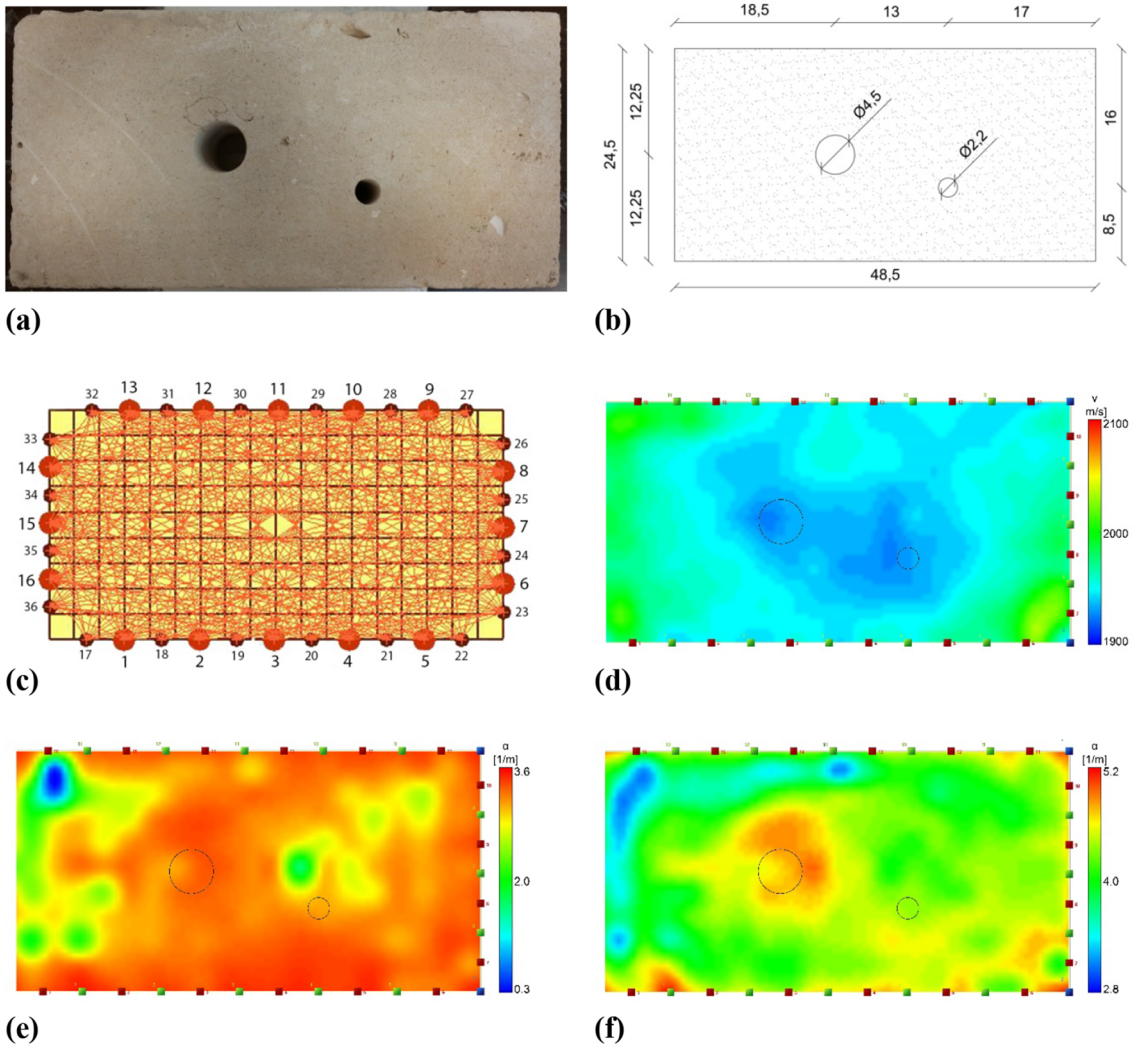

Fig. 7 **a** Picture of the specimen. **b** Relevant dimensions of the specimen and of the defects (cm). **c** Layout of tomographic measurements. **d** TT velocity map (m/s). **e** OAT attenuation map (1/m). **f** SAT attenuation map (1/m)

b). The artificial defects were now two pass-through holes close together and located approximately near the center of the specimen; in particular, the diameter of the hole on the left is 4.5 cm, whereas that of the hole on the right is 2.2 cm. In this case, the aim of the test is that of assessing if the tomographic techniques under investigation can detect and distinguish two different defects with similar geometry, and close to each other. For tomography, 236 measurements were carried out according to the layout shown in Fig. 7c, that also shows the discretization of the cross-section in $9 \times 18 = 162$ pixels.

The obtained results are displayed in Figs. 7d (velocity map obtained by standard TT procedure), 7e (attenuation map obtained by standard OAT procedure) and 7f (attenuation map obtained by the innovative SAT procedure).

Also in Test 4 OAT map (Fig. 7e) is practically uncorrelated to the actual internal morphology. TT gives overall the best results, although the accuracy is quite low (as in the other cases). Indeed, Fig. 7d shows a low-velocity area surrounding the two holes, with lowest velocity values near the exact location of the holes. Anyway, the low-velocity area is much more extended of the actual area containing the holes, interesting also a part of the specimen near the upper edge, where no defects are. Moreover, according to TT map right defect wrongly appears to be bigger than the left defect. SAT map (Fig. 7f) allows for a quite sharp location of the larger hole, whereas the smaller hole is practically not detected, and physically meaningless high attenuation areas are displayed along the edges of the specimen.

The above results are consistent with the considerations made with regards to Test 3, namely that the rather worse quality of TT and SAT results with respect to Test 1 can be justified by the large difference in the hole area: indeed, in

the present case the area of holes is about 48% (the larger) and 11,5% (the smaller) of the area of the hole of Test 1.

About the difficulties of both TT and SAT in accurately characterizing defects, see also the considerations made at the end of Sect. 4.3 about the influence of the dimensions of the defect, also compared to the wavelength, on the detection capability.

Again, TT and SAT appear to have a complementary capability, and this suggests that a possible way for obtaining a more thorough reconstruction of the internal morphology is that of performing both TT and SAT and to find criteria for taking simultaneously into account the results obtained in terms of velocity and attenuation.

5 Conclusions

In this paper, the capability of amplitude ultrasonic tomography (AT) in giving worthwhile information about the internal morphology, and of characterizing internal defects is studied and discussed with tests performed on stone masonry elements. AT is based on amplitude measurements, and the reconstructed parameter is wave attenuation. In theory, the latter is more strictly affected by internal discontinuity and defects; thus, in principle AT is very promising, but its diffusion in the applications is obstructed by several limitations that practically cancel out AT advantages.

To overcome these limitations, here an innovative amplitude ultrasonic tomography approach, called Standardized Amplitude Tomography (SAT), is proposed. SAT is based both on theoretical improvements of the tomographic procedure, concerning the model equation and the determination of the initial amplitude, and on the use of a suitable experimental device, expressly designed and built. It is noteworthy that although the new SAT approach has been developed for masonry structures, and although the reported experimental tests concern masonry elements, the field of application of SAT includes also concrete structures. Moreover, the principle can be easily extended to timber structures.

Experimental results obtained on laboratory specimens with known artificial defects show that SAT can drastically improve the capability of AT. Whereas experiments have been performed on masonry construction materials (tuff blocks), it is clear that similar improvements can be obtained also for other materials like, e.g., concrete and timber.

It is worth noting that in the case-studies discussed in Sect. 4 the improvements of SAT over the standard OAT are only due to the theoretical improvements, since both for OAT and SAT wave measurements are made by using the above recalled special experimental device.

The examined case-studies show that the quality of SAT results is comparable to those obtained by travel time tomography (TT), and in some cases even better.

Generally speaking, SAT has shown sharper results than TT, even if not in all tests all the defects have been detected. On the other hand, also TT proved to be unable to reveal some defects. Indeed, some limitations of TT well known in literature emerged: for example, TT is incapable to find central small low-velocity anomalies.

The difference in terms of the model parameter between TT and SAT suggests that these two tomography approaches have complementary capabilities, and therefore that by employing both TT and SAT it is possible to gather a more accurate overview of the internal morphology of masonry structures. In this vein, notice that referring to other applicative fields some Authors have already proposed to suitably combine travel time and attenuation tomography information [52]. This challenging task will be the object of further investigations, aimed at overcoming a number of theoretical and experimental issues related to the combination of TT and SAT results, and at identifying an effective combination strategy.

The obtained results encourage to further deepen the study and the enhancement of AT approaches suitable for applications to masonry structures: for example, some issues worth of investigation are the calibration of the wavelength of the emitted wave with respect to the expected dimension of the discontinuities in masonry elements, and the enhancement of the model equation proposed in Sect. 3.2 by considering more complex directivity functions valid for describing the spatial distribution of the acoustic pressure generated in isotropic elastic solids by cylindrical transducers. To this aim, it is noteworthy that the knowledge of the ratio between the velocities of longitudinal waves and shear waves is required. Since those velocities are usually unknown in advance, it is possible to overcome the problem by incorporating these parameters in the inversion procedure as additional unknowns.

Finally, the accuracy of SAT results may be further improved by developing ad hoc inversion procedures, which can better manage the inconsistent data gathered on masonry structures. The latter improvement can be fruitfully extended also to TT approaches.

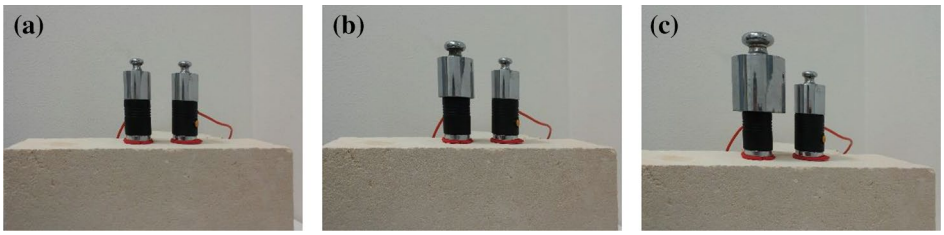

Fig. 8 Experimental tests on the influence on the measured amplitude of the pressure exerted on the transducers: **a**) Test 1 (weight 1 kg); **b** Test 2 (weight 2 kg); **c** Test 3 (weight 5 kg)

Table 1 Results of the experimental tests on the influence on the measured amplitude of the pressure exerted on the transducers

Test 1 (weight 1 kg)		Test 2 (weight 2 kg)		Test 3 (weight 5 kg)	
Mean amplitude (mV)	0.48	Mean amplitude (mV)	0.67	Mean amplitude (mV)	1.16
Range (mV)	0.11	Range (mV)	0.09	Range (mV)	0.17
Standard deviation (mV)	0.03	Standard deviation (mV)	0.02	Standard deviation (mV)	0.04
Coefficient of variation (%)	5.69	Coefficient of variation (%)	3.45	Coefficient of variation (%)	3.43

Appendix: Experimental evaluation of the dependence of the amplitude from the pressure exerted by the transducers

Here, an experimental test for investigating the correlation between the variation of the coupling conditions and the value of the measured amplitude is reported. In particular, the correlation between the pressure exerted by the transducers, both source and receiver, in the investigate surfaces and the measured amplitude has been studied.

In particular, three tests were carried out on a tuff block by using an ultrasonic equipment having a source transducer with peak frequency 55 kHz and a PZT receiver. For all the performed tests a weight with a mass of 1 kg was placed on the top of the source transducer. The three tests differ for the mass of the weight placed on the top of the receiver transducer, which is 1 kg in the first test, 2 kg in the second and 5 kg in the third (see Fig. 8).

Each test consisted of 25 cycles, each composed by a loading phase, in which the receiver transducer was loaded by the weight, and by an unloading phase, in which the weight was removed. The load on the source transducer was constantly maintained. For each cycle, the received wave amplitude was measured at the end of the loading phase. The 25 amplitude values acquired for each test have been statistically processed.

The obtained results, listed in Table 1, clearly show that there exists a marked pressure-amplitude correlation; the values of the coefficient of variation indicate that the value of the measured amplitude becomes as more stable as the load on the transducer increases.

In addition, it is worth noting that for each of the considered values of the weight acting on the receiver transducer, the coefficient of variation evaluated on the 25 acquired values of the amplitude is rather small, ranging from 3.43% to 5.69%. This shows that once leveled the pressure exerted on the transducer, the amplitude can be considered constant within an order of approximation consistent with the approximations typical of the tomographic experiments under investigation.

Finally, the obtained results indicate that also the position of the weight is influential on the measured amplitude: indeed, in order to get reliable measurements, it is necessary that the force exerted on the transducers is centered.

References

1. McCann, D.M., Forde, M.C.: Review of NDT methods in the assessment of concrete and masonry structures. NDT&E Int. **34**, 71–84 (2001)
2. Castellano, A., Fraddosio, A., Martorano, F., Mininno, G., Paparella, F., Piccioni, M.D.: Structural health monitoring of a historic masonry bell tower by radar interferometric measurements. Environ. Energy Struct. Monit. Syst. Proc. (2018). https://doi.org/10.1109/EESMS.2018.8405824
3. Binda, L.: The importance of investigation for the diagnosis of historic buildings: Application at different scales (centres and single buildings). In: Modena, C., Lourenço, P.B, Roca, P., (eds.). Structural Analysis of Masonry Historical Constructions Possibilities Numer. Exp. Tech. – Proceeding of Fourth International Seminars Structure Analysis of Historical Structure, Padova vol. 1, A.A. Balkema Publishers, Leiden, 29–42. (2005)
4. Binda, L., Saisi, A., Tiraboschi, C.: Investigation procedures for the diagnosis of historic masonries. Constr. Build. Mater. (2000). https://doi.org/10.1016/S0950-0618(00)00018-0
5. Binda, L, Saisi, A.: Diagnosis and investigation strategies in the assessment of historic buildings. In: 4th International Congress on Science and Technology for the safeguard of cultural heritage in the Mediterranean. Basin Cairo, 347–56. (2009)
6. Maierhofer, C.: Combination of non-destructive testing methods for the assessment of masonry structures. In: Binda, L., di Prisco,

M., Felicetti, R., (eds.). RILEM Symp. Site Assess. Concr. Mason. Timber Struct.-SACoMaTiS 2008, 715–26. (2008)
7. Rhazi, J.: Evaluation of concrete structures by the acoustic tomography technique. Struct. Health Monit. **5**, 333–342 (2006)
8. Yin, S., Cui, Z., Fu, J., Kundu, T.: Acoustic source localization in heterogeneous media. Ultrasonics (2019). https://doi.org/10.1016/j.ultras.2019.105957
9. Binda, L., Cardani, G., Zanzi, L.: Nondestructive testing evaluation of drying process in flooded full-scale masonry walls. J. Perform. Constr. Facil. (2010). https://doi.org/10.1061/(ASCE)CF.1943-5509.0000097
10. Castellano, A., Foti, P., Fraddosio, A., Marzano, S., Piccioni, M.D.: Ultrasonic immersion tests for mechanical characterization of multilayered anisotropic materials. In: EESMS 2014–2014 IEEE Work. Environmental, Energy, and Structural Monitoring Systems 2014.https://doi.org/10.1109/EESMS.2014.6923266.
11. Vasconcelos, G., Lourenço, P.B., Alves, C.A.S., Pamplona, J.: Ultrasonic evaluation of the physical and mechanical properties of granites. Ultrasonics (2008). https://doi.org/10.1016/j.ultras.2008.03.008
12. Castellano, A., Foti, P., Fraddosio, A., Galietti, U., Marzano, S., Piccioni, M.D.: Characterization of material damage by ultrasonic immersion test. Procedia Eng. (2015). https://doi.org/10.1016/j.proeng.2015.06.248
13. Castellano, A., Foti, P., Fraddosio, A., Marzano, S., Paparella, F., Piccioni, M.D.: Monitoring applied and residual stress in materials and structures by non-destructive acoustoelastic techniques. In: EESMS 2016–2016 IEEE Work. Environmental, Energy, and Structural Monitoring Systems (2016). https://doi.org/10.1109/EESMS.2016.7504830.
14. Castellano, A., Fraddosio, A., Marzano, S., Piccioni, M.D.: Some advancements in the ultrasonic evaluation of initial stress states by the analysis of the acoustoelastic effect. Procedia Eng. (2017). https://doi.org/10.1016/j.proeng.2017.09.494
15. Binda, L., Saisi, A., Zanzi, L.: Sonic tomography and flat-jack tests as complementary investigation procedures for the stone pillars of the temple of S Nicolò 1'Arena (Italy). NDT&E Int (2003). https://doi.org/10.1016/S0963-8695(02)00066-X
16. Leucci, G., Masini, N., Persico, R., Soldovieri, F.: GPR and sonic tomography for structural restoration: the case of the cathedral of Tricarico. J. Geophy.s Eng. (2011). https://doi.org/10.1088/1742-2132/8/3/S08
17. Wendrich, A., Trela, C., Krause, M., Maierhofer, C., Effner, U., Wöstmann, J:. Location of voids in masonry structures by using radar and ultrasonic traveltime tomography. In: ECNDT 2006, 9th European Conference Non-Destructive Testing, Berlin, DE, 2006.
18. Colla, C., Gabrielli, E.: On-site diagnosis of masonry structures via sonic tomography: The case of the ex-church of San Barbaziano. In: Modena, C., da Porto, F.V.M.R (eds.). Brick Block Mason. Trends, Innov. Challenges—Proceeding of 16th International Brick Block Mason. Conference of IBMAC 2016, CRC Press/Balkema, 1507–1514, (2016)
19. Silva, B., Dalla Benetta, M., Da Porto, F., Valluzzi, M.R.: Compression and sonic tests to assess effectiveness of grout injection on three-leaf stone masonry walls. Int. J. Archit. Herit. (2014). https://doi.org/10.1080/15583058.2013.826300
20. Luchin, G., Ramos, L.F., D'Amato, M.: Sonic tomography for masonry walls characterization. Int. J. Archit. Herit. (2018). https://doi.org/10.1080/15583058.2018.1554723
21. Valluzzi, M.R., Cescatti, E., Cardani, G., Cantini, L., Zanzi, L., Colla, C., et al.: Calibration of sonic pulse velocity tests for detection of variable conditions in masonry walls. Constr. Build. Mater. (2018). https://doi.org/10.1016/j.conbuildmat.2018.10.073
22. Zielińska, M., Rucka, M.: Non-destructive assessment of masonry pillars using ultrasonic tomography. Materials (Basel) (2018). https://doi.org/10.3390/ma11122543
23. Dackermann, U., Crews, K., Kasal, B., Li, J., Riggio, M., Rinn, F., et al.: In situ assessment of structural timber using stress-wave measurements. Mater. Struct. Constr. (2014). https://doi.org/10.1617/s11527-013-0095-4
24. Riggio, M., Macchioni, N., Riminesi, C.: Structural health assessment of historical timber structures combining non-destructive techniques: the roof of Giotto's bell tower in Florence. Struct. Control Health Monit. (2017). https://doi.org/10.1002/stc.1935
25. Schabowicz, K.: Ultrasonic tomography - The latest nondestructive technique for testing concrete members - Description, test methodology, application example. Arch. Civ. Mech. Eng. (2014). https://doi.org/10.1016/j.acme.2013.10.006
26. Choi, H., Popovics, J.S.: NDE application of ultrasonic tomography to a full-scale concrete structure. IEEE Trans. Ultrason Ferroelectr. Freq. Control (2015). https://doi.org/10.1109/TUFFC.2014.006962
27. Choi, H., Ham, Y., Popovics, J.S.: Integrated visualization for reinforced concrete using ultrasonic tomography and image-based 3-D reconstruction. Constr. Build. Mater. (2016). https://doi.org/10.1016/j.conbuildmat.2016.07.010
28. Colla, C., Grüner, F., Dieruff, B., Fiedler, K., Pascale, G., Gabrielli, E. et al. SMooHS: Smart Monitoring of Historic Structures D5.1-part 1 Report on test methods and former test results. (2010).
29. Concu, G., DeNicolo, B., Piga, C., Popescu, V.: Non-destructive testing of stone masonry using acoustic attenuation tomography imaging. In: Proceeding of the 12th International Conference on Civil, Structural and Environmental Engineering Computing. Civil-Comp Press; (2009)
30. Hudson, J.A.: Wave speeds and attenuation of elastic waves in material containing cracks. Geophys. J. R. Astron. Soc. **64**, 133–150 (1981)
31. Quan, Y., Harris, J.M.: Seismic attenuation tomography using the frequency shift method. Geophysics **62**, 895–905 (1997)
32. Wang. Seismic Amplitude Inversion in Reflection Tomography. (2003).
33. Nolet, G.: A breviary of seismic tomography. Imaging Inter. (2008). https://doi.org/10.1017/CBO9780511984709.
34. DeNicolo, B., Piga, C., Popescu, V., Concu, G.: Non invasive acoustic measurements for faults detecting in building materials and structures. In: Haq, M.Z. (ed.). Application of Measurement Systems. IntechOpen, Rijeka, 259–292 (2012,).
35. Prada, J., Fratta, D., Santamarina, J.C.: Tomographic Detection of Low-Velocity Anomalies with Limited Data Sets (Velocity and Attenuation). Geotech Test J **23**, 472–486 (2000)
36. Chai, H.K., Momoki, S., Kobayashi, Y., Aggelis, D.G., Shiotani, T.: Tomographic reconstruction for concrete using attenuation of ultrasound. NDT&E Int. (2011). https://doi.org/10.1016/j.ndteint.2010.11.003
37. Chai, H.K., Liu, K.F., Behnia, A., Yoshikazu, K., Shiotani, T.: Development of a tomography technique for assessment of the material condition of concrete using optimized elastic wave parameters. Materials (Basel) (2016). https://doi.org/10.3390/ma9040291
38. Núñez, D.L., Molero-Armenta, M.Á., Izquierdo, M.Á.G., Hernández, M.G., Velayos, J.J.A.: Ultrasound transmission tomography for detecting and measuring cylindrical objects embedded in concrete. Sensors (Switzerland) (2017). https://doi.org/10.3390/s17051085
39. Choi, H., Popovics, J.S.: Application of semi-coupled ultrasonic pulse velocity to image concrete structures using tomographic

algorithms. IEEE International Ultrasonics Symposium IUS, (2014). https://doi.org/10.1109/ULTSYM.2014.0249.
40. Hall, K.S., Popovics, J.S.: Air-coupled ultrasonic tomography of solids: 2 application to concrete elements. Smart. Struct. Syst. (2016). https://doi.org/10.12989/sss.2016.17.1.031
41. Camassa, D., Castellano, A., Fraddosio, A., Piccioni, M.D.: Improvements of the ultrasonic tomography for applications to historical masonry constructions. In: Aguilar, R., Torrealva, D., Moreira, S., Pando, M.A.R.L.F (eds.). Structural Analysis of Historic Construction. RILEM Bookseries, vol. 18, Springer, 447–455 (2019).
42. Menke, W.: Geophysical Data Analysis: Discrete Inverse Theory. Academic Press, Amsterdam (2012)
43. Tarantola, A.: Inverse Problem Theory and Methods for Model Parameter Estimation. Society for Industrial and Applied Mathematics, Philadelphia (2005)
44. Santamarina, J.C., Fratta, D.: Discrete Signals and Inverse Problems: An Introduction for Engineers and Scientists. Wiley, Hoboken (2005)
45. Červený, V.: Seismic ray theory. J. Seismol. **7**, 543–543 (2003)
46. Berryman, J.G.: Lecture notes on nonlinear inversion and tomography; I, borehole seismic tomography. 1991.
47. Gheshlaghi, F.: Tomographic imaging in civil engineering infrastructure. University of Waterloo, Waterloo (1997)
48. Lehmann, B.: Seismic traveltime tomography for engineering and exploration applications. EAGE publications, Houten (2007)
49. Rose, J.L.: Ultrasonic Waves in Solid Media. Cambridge University Press, Cambridge (2008)
50. Cheeke, J.D.N.: Fundamentals and Applications of Ultrasonic Waves. CRC Press, Boca Raton (2002)
51. Kinsler, L.E., Frey, A.R., Coppens, A.B., Sanders, J.V.: Fundamentals of acoustics 4th edition. (2000).
52. Dębski, W., Young, R.P.: Enhanced velocity tomography: practical method of combining velocity and attenuation parameters. Geophys. Res. Lett. (1999). https://doi.org/10.1029/1999GL010368